polymers

MDPI

Article

Thermal Effect and Mechanism Analysis of Flame-Retardant Modified Polymer Electrolyte for Lithium-Ion Battery

Zhi-Hao Wu [1], An-Chi Huang [1,*], Yan Tang [1,*], Ya-Ping Yang [2], Ye-Cheng Liu [2], Zhi-Ping Li [1], Hai-Lin Zhou [1], Chung-Fu Huang [3], Zhi-Xiang Xing [1,*], Chi-Min Shu [4] and Jun-Cheng Jiang [1,*]

1 School of Environmental and Safety Engineering, Changzhou University, Changzhou 213164, China; 19083700144@smail.cczu.edu.cn (Z.-H.W.); 19083700288@smail.cczu.edu.cn (Z.-P.L.); 19083700424@smail.cczu.edu.cn (H.-L.Z.)
2 School of Material Science and Engineering, Changzhou University, Changzhou 213164, China; B1900012@smail.cczu.edu.cn (Y.-P.Y.); B20080526@smail.cczu.edu.cn (Y.-C.L.)
3 School of Environmental and Chemical Engineering, Zhaoqing University, Zhaoqing 526061, China; huangchungfu@gmail.com
4 Department of Safety, Health, and Environmental Engineering, National Yunlin University of Science and Technology, Yunlin 64002, Taiwan; shucm@yuntech.edu.tw
* Correspondence: huangac@cczu.edu.cn (A.-C.H.); tycd@cczu.edu.cn (Y.T.); xingzhixiang@cczu.edu.cn (Z.-X.X.); jiangjuncheng@cczu.edu.cn (J.-C.J.)

Abstract: In recent years, the prosperous electric vehicle industry has contributed to the rapid development of lithium-ion batteries. However, the increase in the energy density of lithium-ion batteries has also created more pressing safety concerns. The emergence of a new flame-retardant material with the additive ethoxy (pentafluoro) cyclotriphosphazene can ameliorate the performance of lithium-ion batteries while ensuring their safety. The present study proposes a new polymer composite flame-retardant electrolyte and adopts differential scanning calorimetry (DSC) and accelerating rate calorimetry to investigate its thermal effect. The study found that the heating rate is positively correlated with the onset temperature, peak temperature, and endset temperature of the endothermic peak. The flame-retardant modified polymer electrolyte for new lithium-ion batteries has better thermal stability than traditional lithium-ion battery electrolytes. Three non-isothermal methods (Kissinger; Kissinger–Akahira–Sunose; and Flynn–Wall–Ozawa) were also used to calculate the kinetic parameters based on the DSC experimental data. The apparent activation energy results of the three non-isothermal methods were averaged as 54.16 kJ/mol. The research results can provide valuable references for the selection and preparation of flame-retardant additives in lithium-ion batteries.

Keywords: lithium-ion battery; ethoxy (pentafluoro) cyclotriphosphazene; polymer composite; flame-retardant electrolyte; thermal stability

Citation: Wu, Z.-H.; Huang, A.-C.; Tang, Y.; Yang, Y.-P.; Liu, Y.-C.; Li, Z.-P.; Zhou, H.-L.; Huang, C.-F.; Xing, Z.-X.; Shu, C.-M.; et al. Thermal Effect and Mechanism Analysis of Flame-Retardant Modified Polymer Electrolyte for Lithium-Ion Battery. *Polymers* **2021**, *13*, 1675. https://doi.org/10.3390/polym13111675

Academic Editors: Didier Devaux, Fannie Alloin, Renaud Bouchet, Cristina Iojoiu and Lauréline Lecarme

Received: 27 April 2021
Accepted: 18 May 2021
Published: 21 May 2021

1. Introduction

With the rapid development of the electric vehicle industry, more attention has been paid to the endurance of lithium-ion batteries in recent years. Accordingly, high requirements have been established for the energy density of lithium-ion batteries in the electric vehicle market. However, high-energy-density lithium-ion batteries generate substantial heat when releasing energy, which leads to a high risk of thermal runaway. In recent years, accidents involving the spontaneous combustion of electric vehicles have occurred frequently [1–3]. On 7 January 2021, a workshop operated by a subsidiary company of Contemporary Amperex Technology Co. exploded due to the thermal runaway of battery waste, resulting in a giant mushroom cloud. Therefore, to enhance the lithium-ion batteries' essential safety, research on the intrinsic safety of lithium-ion batteries is eagerly demanded. At present, scholars have developed solid-state electrolyte lithium-ion batteries that are safer than liquid-state ones. However, the current solid-state electrolyte lithium-ion

batteries face problems, such as short battery cycle life, high solid–solid interface contact resistance, and poor interface compatibility and stability [4]. Nowadays, lithium-ion batteries on the market consist of positive and negative electrodes coated with highly active electrode materials, separators, and electrolytes. To solve the thermal safety problems of lithium-ion batteries, the design and development of electrolyte flame-retardant additives are critical. Adding electrolyte flame-retardant additives is currently one of the most economical and effective methods to reduce the thermal runaway risk of lithium-ion batteries because of their low cost and high performance [5–7].

At present, the chief flame-retardant additives include phosphate esters, fluorinated ring triphosphazene, and organic halogenated compounds. In the past few years, phosphate ester flame-retardant additives have shown excellent flame-retardant effects but low electrochemical performance in lithium-ion batteries [8]. Flame-retardant additives derived from organic halogenated compounds are environmentally unfriendly. Furthermore, phosphate esters and organic halogenated compounds need to be added with about 10.0 mass% or more to make the electrolyte non-flammable [9]. Fluorinated ring triphosphazene flame-retardant additives have attracted the attention of researchers because they only need to be added with 5.0 mass% to make the electrolyte non-flammable, and they do not affect electrochemical performance [10–12].

Recently, various derivatives of fluorinated ring triphosphazene have been discovered. A new flame-retardant additive, ethoxy (pentafluoro) cyclotriphosphazene (PFPN), has been proposed by researchers. The research into PFPN mainly focuses on the self-extinguishing time (SET) test and the electrochemical performance test of the PFPN as an electrolyte additive of the lithium-ion battery. Lan has indicated that the PFPN additive has sufficient electrochemical compatibility with the graphite anode and improved the cycling performance of the positive electrode of the lithium-ion battery through charge and discharge tests [13]. Liu has pointed out that PFPN can improve the cycle stability of a lithium nickel manganese oxide ($LiNi_{0.5}Mn_{1.5}O_4$) cathode and has a flame-retardant effect [14]. Using SET and critical oxygen index tests, it has become clear that PFPN can reduce electrode polarization and enhance the electrochemical performance of $LiCoO_2$ electrodes [15].

However, few researchers have analyzed the thermal hazard and thermal stability of PFPN electrolytes. It is necessary to investigate the thermal properties of lithium-ion battery electrolytes. Hence, in the present paper, differential scanning calorimetry (DSC) and accelerating rate calorimetry (ARC) were used to conduct thermal analyses on standard lithium-ion battery electrolytes and PFPN-added new polymer composite lithium-ion battery electrolytes [16–18]. The flame retardancy of PFPN and the thermal stability of PFPN at different temperatures were also analyzed. Based on experimental data, we carried out simulations to determine the thermal decomposition mechanism of PFPN and used different non-isothermal methods to calculate its thermokinetic parameters. According to the experimental results and the thermokinetic models (Kissinger, Kissinger–Akahira–Sunose (KAS), and Flynn–Wall–Ozawa (FWO)), the apparent activation energy (E_a) was then calculated.

2. Materials and Methods

2.1. Chemicals and Materials

All chemicals and materials were purchased from commercial sources (Battery grade, Aldrich Co.) and used directly without further purification. As an electrolyte salt, lithium hexafluorophosphate ($LiPF_6$) has excellent ionic conductivity, solid electrolyte interface (SEI) film formation, and corrosion resistance. At the same time, the nature of the organic solvent in lithium-ion battery electrolytes often determines the nature of the electrolyte. In order to form a high-quality SEI film that is more easily reduced at low potential, ethylene carbonate (EC) with a ring structure and dimethyl carbonate (DMC) with a low viscosity are very good choices. The initial characteristics of common lithium-ion battery electrolyte solvents are shown in Table 1 [19,20]. This experiment used commercial electrolyte LP30

(1.0 M, $LiPF_6$ dissolved into a 1:1 (by volume) mixture of EC and DMC) as the standard electrolyte. The literature indicated that the flame-retardant and electrochemical performance of adding 5.0 mass% cyclotriphosphazene flame-retardant additives is the best [13,15]. Therefore, 5.0 mass% PFPN (>98 mass%, TCI) was selected to be added to the standard electrolyte as a flame-retardant electrolyte. Both electrolytes are configured in a glove box (JMS-S1X, Nanjing Jiumen Automation Technology Co., Nanjing, China) with a water and oxygen content of less than 0.2 ppm. An argon atmosphere was used to prevent the electrolyte from reacting with oxygen and water in the air.

Table 1. The initial characterization of common lithium-ion battery electrolyte solvents.

Organic Solvent	Boiling Point (°C)	Flash Point (°C)	Melting Point (°C)	Viscosity (mPa·s) (25 °C)	Dielectric Constant
Ethylene carbonate (EC)	248	160	37	1.90	89.6
Dimethyl carbonate (DMC)	90	17	2	0.62	2.6
Propylene carbonate (PC)	242	128	−49	2.50	69.0
Diethyl carbonate (DEC)	126	25	−43	0.75	2.8
Ethyl methyl carbonate (EMC)	108	23	−55	0.65	2.9

2.2. Adiabatic Reaction Calorimetry (ARC) Measurement

Studies have shown that PFPN has sound flame-retardant properties, but the thermal behavior and thermal parameters are unclear [13,15]. ARC (ARC254, NETZSCH-Gerätebau GmbH Co., Selb, Germany) experiments were performed on the standard electrolyte and the flame-retardant electrolyte to obtain the thermokinetic parameters and reaction heat of PFPN in the electrolyte under the adiabatic state. The tested electrolyte sample was inserted into a titanium alloy ball, sealed with a thin film, and the operations were carried out in the glove box. The net weight was controlled at 3.0 ± 0.5 g. We selected the heat–wait–search mode for adiabatic testing from the ARC experiments settings. The sample was swiftly heated to 80.0 °C from the room temperature at which the experiment started, and then the temperature was equilibrated for 30.0 min to test the heat release. When the self-heating rate was less than 0.02 °C/min, there was determined to be no exothermal process at that temperature, and then a 5.0 °C increase in temperature was carried out at a rate of 10.0 °C/min to test the exotherm again. If an exothermic reaction was detected, the system adapted the external environment temperature to make it consistent with the reaction system temperature and achieve the pseudo-adiabatic effect. When the temperature reached 350.0 °C, the heat–wait–search mode ended, and the temperature and pressure changes of the reaction system under the adiabatic state were obtained [21].

2.3. Differential Scanning Calorimetry (DSC) Measurement

To strengthen the validity of the experimental data measured from ARC, we used the DSC instrument (HP DSC3, Mettler-Toledo Co., Zurich, Switzerland) to examine the standard electrolyte and PFPN-added flame-retardant electrolyte. The obtained specific exothermic characteristics of the new polymer composite flame-retardant electrolyte were further combined with thermokinetic models. The two electrolyte solutions were put into the aluminum DSC sample pan and sealed in a glove box filled with argon gas to prevent external moisture and oxygen from contacting the electrolyte. The net electrolyte content in the sample pan was 6.5 ± 0.5 mg. The samples were heated from 30 to 350 °C at heating rates of 1, 2, 4, 7, and 10 °C/min [22–26]. By comparing the thermal stability parameters (initial reaction temperature (T_o), peak temperature (T_p), and end reaction temperature (T_e), the thermal behavior of the standard electrolyte and flame-retardant electrolyte were evaluated [27–30].

2.4. Kinetic Analysis

Utilizing the thermokinetic models to determine E_a is a reliable method to reveal electrolyte thermal safety and mechanisms. Based on the thermodynamic data obtained

from the DSC experiments, the present paper used the iso-conversional rate method to calculate the thermokinetic parameters of electrolytes. Given that the data were obtained at the same conversion rate (α) under different heating rates (β) in the same experiment, the E_a obtained is relatively reliable [31,32]. The present study used three model-free non-isothermal methods (Kissinger, KAS, and FWO) to calculate the E_a of the essential electrolyte and the flame-retardant electrolyte. The thermal safety evaluation of PFPN in the electrolyte can be better evaluated by comparing the calculation results.

2.4.1. Kissinger Model

The Kissinger method, also known as the maximum method, is applicable for processes that occur under linear heating rate conditions. Given its convenience, it is the most widely used conversion rate method [33–36]. The method is shown as the following Equation (1):

$$\ln\left(\frac{\beta}{T^2}\right) = \ln\left[-\frac{AR}{E_a}f'(\alpha)\right] - \frac{E_a}{RT} \quad (1)$$

where A is the pre-exponential factor; T is the reaction temperature, K; $f(\alpha)$ is the mechanism function, $f'(\alpha) = \mathrm{d}f(\alpha)/\mathrm{d}\alpha$; R is the ideal gas constant, R = 8.314 J/(mol·K); and E_a is an exact value only when $f'(\alpha)$ is a constant. Therefore, $f'(\alpha)$ needs to be independent of the heating rate.

2.4.2. KAS Method

Using the Coats–Redfern approximation of the temperature integral, the KAS equation was derived. As a conversion rate method, the KAS method improves the accuracy of calculating E_a [32,33,37]. As shown in the following Equation (2):

$$\ln\left(\frac{\beta}{T^2}\right) = \ln\left[\frac{AR}{E_a G(\alpha)}\right] - \frac{E_a}{RT} \quad (2)$$

where $G(\alpha)$ is the reaction function.

2.4.3. FWO Method

This method calculates the same reaction at different heating rates; when α is the same value, the $G(\alpha)$ is specific [33,38–40], as shown in the following Equation (3):

$$\ln\beta = \ln\left[\frac{AE_a}{RG(\alpha)}\right] - 2.315 - 0.4567\frac{E_a}{RT} \quad (3)$$

When α is appointed, the corresponding T can be calculated. Therefore, a fixed α has corresponding T and β values. Then E_a can be calculated according to the above formula. In this method, the error caused by mechanism functions can be avoided because E_a is obtained directly without utilizing these functions.

3. Results and Discussion

3.1. Analysis of Results

The DSC calorimetry results of LP30 and LP30 + PFPN are shown in Table 2, and Figures 1 and 2. With the increase in β, the T_o, T_p, and T_e in the endothermic peaks of LP30 and LP30 + PFPN increased. With the increase in temperature, two endothermic peaks occurred for LP30 and LP30 + PFPN. The two endothermic peaks of LP30 appeared between 68.67 and 158.33 °C and 192.67 and 258.67 °C. The two endothermic peaks of LP30 + PFPN appeared between 61.33 and 159.33 °C and 178.67 and 260.67 °C. According to the literature, the reason for the first endothermic peak is the decomposition of $LiPF_6$, which decomposes into LiF solid and PF_5 gas in an inert environment [41,42]. The reason for the second endothermic peak is the evaporation of the solvent in the electrolyte. The first peak range is smaller than the second one, indicating that $LiPF_6$ requires less energy to decompose, and it is easier to react. As shown in Figure 3, at the same heating rate, the

areas of the two endothermic peaks became more significant after adding PFPN, indicating that the reaction heats of the two reactions had become more intense. Besides this, the endothermic peak temperature range widened, implying that the endothermic reaction commenced earlier and the reaction system was safer than the original LP30. It can be inferred from this that PFPN can make the LP30 electrolyte more stable.

Table 2. Characteristic parameters of LP30 and LP30 + PFPN.

β (°C/min)	Mass (mg)	LP30						LP30 + PFPN					
		T_{o1} (°C)	T_{p1} (°C)	T_{e1} (°C)	T_{o2} (°C)	T_{p2} (°C)	T_{e2} (°C)	T_{o1} (°C)	T_{p1} (°C)	T_{e1} (°C)	T_{o2} (°C)	T_{p2} (°C)	T_{e2} (°C)
1	6.5 ± 0.5	68.67	103.33	132.33	192.67	223.00	260.33	61.33	96.67	140.33	178.67	222.00	272.67
2		78.67	103.33	123.33	191.67	223.00	258.00	56.00	97.67	137.00	162.33	200.00	248.67
4		89.00	104.67	122.00	193.33	239.67	262.33	81.33	105.33	129.67	183.00	234.00	264.00
7		95.45	117.85	146.55	195.90	212.70	234.47	95.45	121.00	150.058	196.25	214.10	236.85
10		121.67	140.67	158.33	202.33	234.67	258.67	122.00	139.00	159.33	204.33	233.67	260.67

T_1 represents the first endothermic peak; T_2 represents the second endothermic peak.

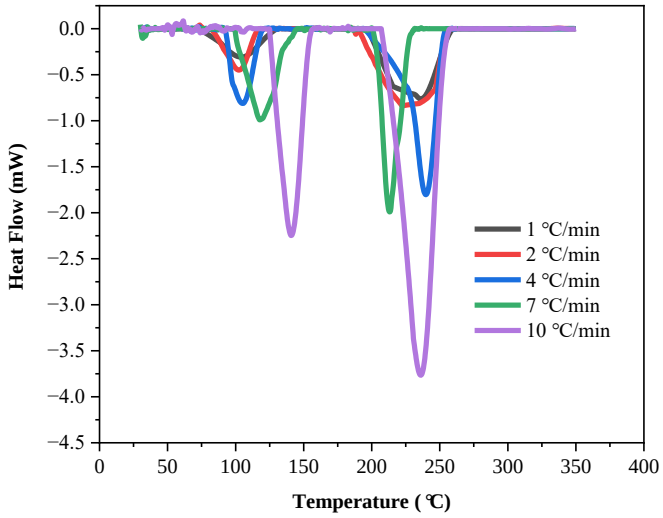

Figure 1. Endothermic curves of LP30 at different heating rates.

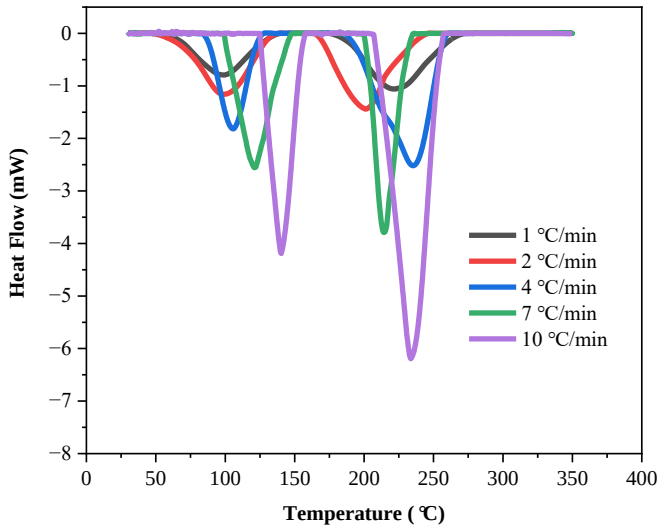

Figure 2. Endothermic curves of LP30 + PFPN at different heating rates.

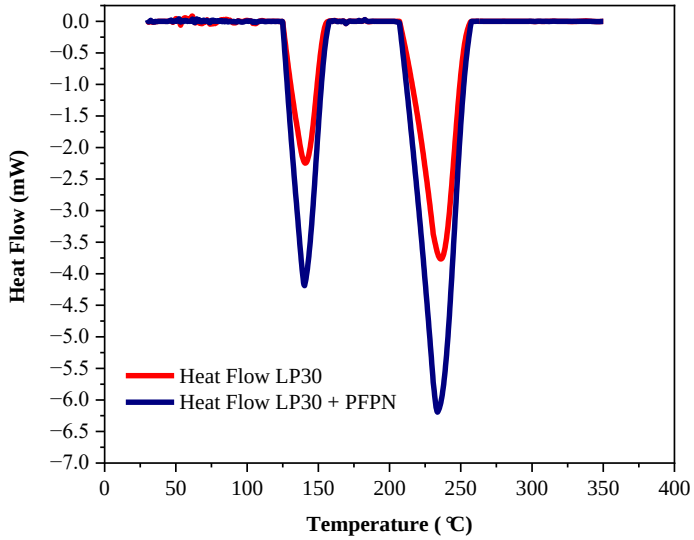

Figure 3. Endothermic curves of LP30 and LP30 + PFPN at β of 10 °C/min.

To further analyze the thermal decomposition behavior of the LP30 + PFPN electrolyte, we conducted an ARC experiment under pseudo-adiabatic conditions. The characteristic parameters of the experiment are listed in Table 3. As illustrated in Figures 4 and 5, when the experiment had progressed by about 1180 min, the temperature of the reaction system reached about 220 °C. At this time, the temperature of the reaction system began to rise, and the pressure also increased. As shown in Figures 6 and 7, when the experiment had been carried out for about 1225 min, the temperature of the reaction system reached about 231 °C, and the pressure reached approximately 70 bar. At this time, the heating rate and pressure rise rate reached their peak values, which were 0.51 °C/min and 1.2 bar/min, respectively.

Table 3. ARC test parameters for LP30 + PFPN.

m_s (g)	m_{ball} (g)	Material	Temperature (°C)	Heating Rate (°C/min)	Exothern Threshold (°C/min)	Waiting Time (min)	Temperature Increment (°C)
3.346	21.000	Hastelloy	80–350	10	0.02	30	5

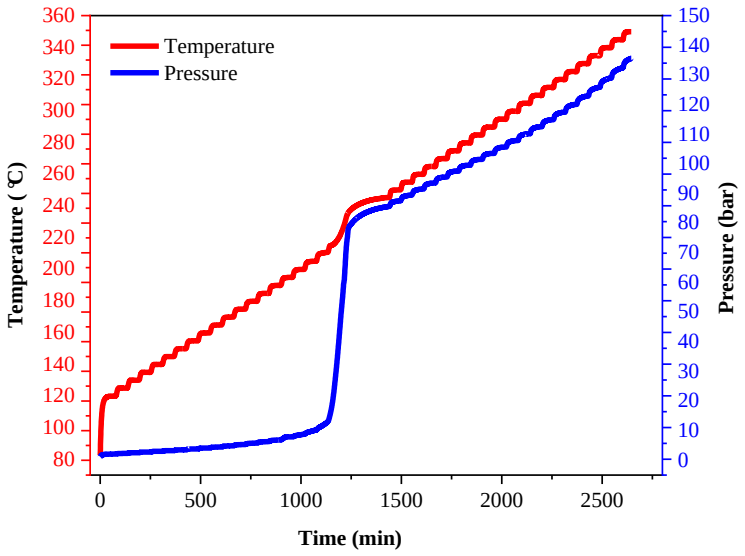

Figure 4. Temperature and pressure versus time (0–2700 min) curves of LP30 + PFPN.

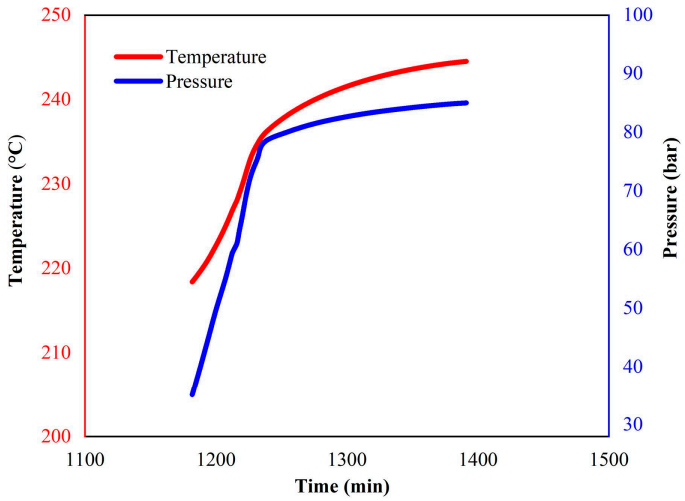

Figure 5. Temperature and pressure versus time (1180–1400 min) curves of LP30 + PFPN.

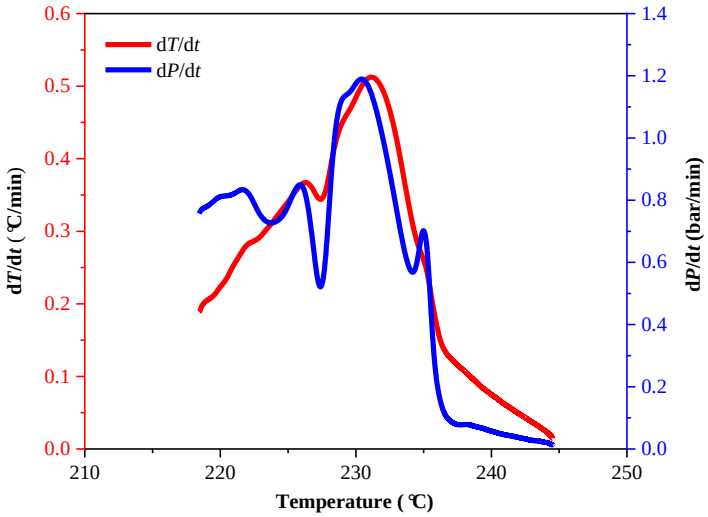

Figure 6. Temperature rise rate and pressure rise rate versus temperature curves of LP30 + PFPN.

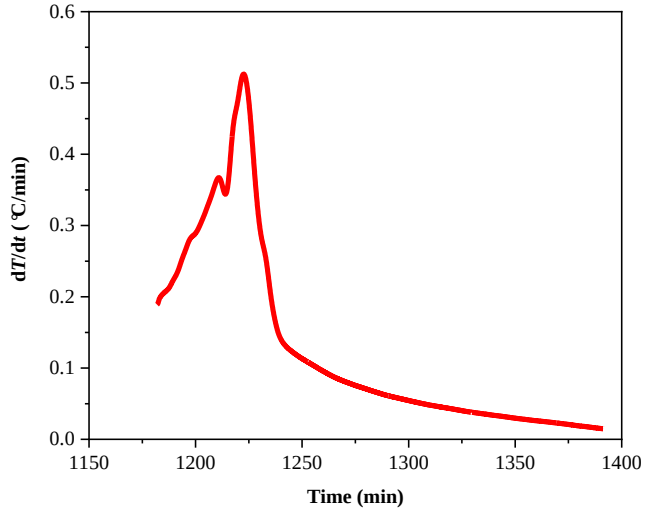

Figure 7. Temperature rise rate time curve of LP30 + PFPN.

The increase in pressure is caused by the vaporization of the solvent in the LP30 + PFPN electrolyte. The temperature at which the pressure in the reaction system started to increase is consistent with the temperature range of the second endothermic peak in the DSC experiment. Because the reaction system is in a pseudo-adiabatic environment, and there is negligible heat loss, it is reasonable to increase the temperature slowly from 220 to 245 °C.

3.2. Analysis of Thermodynamic Results

The interior of the lithium-ion battery system is not an adiabatic environment; therefore, this article discussed the effect of PFPN on the thermal stability of LP30. A kinetic model was established, and the kinetic parameters were calculated based on the data of the first endothermic peak in the DSC experiments.

The International Congress on Thermal Analysis and Calorimetry pointed out that the data obtained from multiple heating rates are reliable for thermokinetic establishment. It is also recommended to use the equal conversion rate method to calculate the reaction kinetics [33]. Therefore, we employed the three models of Kissinger, KAS, and FWO to calculate the E_a through the DSC experimental data at different heating rates (β = 1, 2, 4, 7, and 10 °C/min). Thereby, mutual authentications were realized based on the accuracy of the E_a values. For both KAS and FWO methods, since the choice of baseline is subjective during analysis, we deliberately chose 12 conversion degree values (α = 0.05, 0.1, 0.2, 0.3, 0.4, 0.5, 0.6, 0.7, 0.8, 0.9, 0.95, and 0.99) for thermokinetic analysis [43,44]. Figure 8 shows the fitting results based on the Kissinger model using the linear relationship between l n (β/T^2) and $1000/T$. The calculation results show that E_a was 50.8878 kJ/mol and the determination coefficient R^2 was 0.9948. Figure 9 shows the corresponding E_a and determination coefficient (R^2) based on the KAS model at different conversion degrees. Then, average values were obtained as $\overline{E}_a$ = 54.1431 kJ/mol and $\overline{R}^2$ = 0.9970. Figure 10 demonstrates the fitting results using the linear relationship between l g (β) and $1000/T$ at different conversion degrees based on the FWO model. Table 4 showcases the values of E_a and R^2 calculated based on the fitting results under different conversion degrees of the FWO model. The average values were also obtained as $\overline{E}_a$ = 57.4436 kJ/mol and $\overline{R}^2$ = 0.9967. Table 5 displays the E_a and R^2 calculated by the three models. The R^2 values calculated by the three models were all approaching 1.0, and the E_a values showed a slight difference, indicating that the E_a calculated using the three models is relatively reasonable. In conclusion, E_a can be determined to be 54.1582 kJ/mol by calculating the average of the three values.

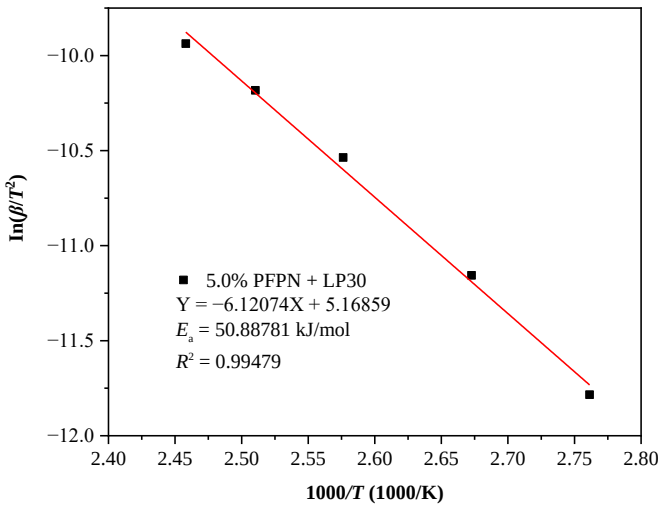

Figure 8. E_a plots of Kissinger model at different β in DSC experiments for LP30 + PFPN.

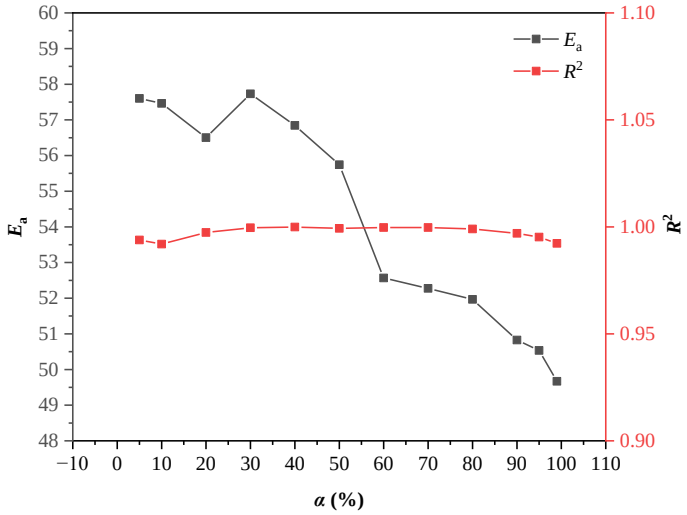

Figure 9. In the DSC experiment, when β is equal to 1, 2, 4, 7, and 10 °C/min, the α-E_a and α-R^2 polyline of LP30 + PFPN under the KAS model.

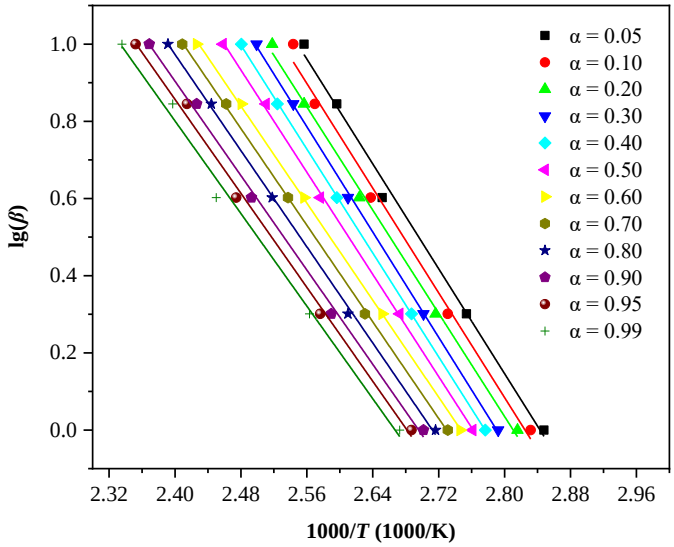

Figure 10. In the DSC experiment, when β is equal to 1, 2, 4, 7, and 10 °C/min, differential isoconversional analysis of LP30 + PFPN under the FWO model.

Table 4. E_a and R^2 under different α based on the FWO model.

α	E_a (kJ/mol)	R^2
0.05	60.5039	0.9931
0.1	60.4064	0.9909
0.2	59.5369	0.9969
0.3	60.7497	0.9995
0.4	59.9467	0.9999
0.5	58.9380	0.9992
0.6	55.9757	0.9997
0.7	55.7361	0.9996
0.8	55.4792	0.9988
0.9	54.4398	0.9966
0.95	54.1983	0.9948
0.99	53.4124	0.9917

Table 5. $\overline{E}_a$ and R^2 values obtained by Kissinger, KAS and FWO methods.

	$\overline{E}_a$ (kJ/mol)	$\overline{R}^2$
Kissinger	50.8878	0.9948
KAS	54.1431	0.9970
FWO	57.4436	0.9967

4. Conclusions

Using the self-synthesized new polymer composite flame-retardant electrolyte, a series of DSC and ARC calorimetry experiments were carried out. Furthermore, a variety of iso-conversion degree models were adopted to calculate the thermodynamic parameters of the new flame-retardant electrolyte. We analyzed the thermal decomposition of LP30 + PFPN and the influence of the flame-retardant additive, PFPN, on the thermal stability of the electrolyte. The experimental results of DSC showed that the values of T_o, T_p, and T_e are obviously affected by β and have a positive relationship with the value of β. In an argon atmosphere, $LiPF_6$ in the new flame-retardant electrolyte decomposed into LiF solid and PF_5 gas at ca. 100 °C, and the addition of PFPN can ameliorate the thermal stability of the electrolyte. Three models—Kissinger, KAS, and FWO, were used to calculate the E_a of LP30 + PFPN, and the calculated results were adjacent, in that R^2 values approached 1. The E_a results of the three methods were averaged as 54.16 kJ/mol. Therefore, the PFPN-added new polymer composite flame-retardant lithium-ion battery electrolyte has better thermal stability than standard electrolytes.

Author Contributions: Conceptualization, Z.-H.W. and A.-C.H.; methodology, A.-C.H. and Y.T.; software, Y.-C.L.; validation, Y.-P.Y.; formal analysis, Z.-H.W. and Y.-C.L.; investigation, H.-L.Z. and Z.-P.L.; resources, Y.T.; data curation, H.-L.Z. and Z.-P.L.; writing—original draft preparation, Z.-H.W.; writing—review and editing, A.-C.H., Y.T. and C.-M.S.; supervision, C.-M.S., C.-F.H., Z.-X.X. and J.-C.J.; project administration, C.-M.S. and C.-F.H.; funding acquisition, Z.-X.X. and J.-C.J. All authors have read and agreed to the published version of the manuscript.

Funding: This research was funded by National Nature Science Foundation of China, grant number 21927815 and 51574046, National Key Research Development Program of China, grant number 2019YFC0810701, and Jiangsu Province Postgraduate Research and Practice Innovation Project.

Institutional Review Board Statement: Not applicable.

Informed Consent Statement: Not applicable.

Data Availability Statement: The data presented in this study are available on request from the corresponding author.

Acknowledgments: The authors thank the experimental and technical support given by Xi-Lin Dong.

Conflicts of Interest: The authors declare no conflict of interest.

References

1. Yuan, M.; Liu, K. Rational design on separators and liquid electrolytes for safer lithium-ion batteries. *J. Energy Chem.* **2020**, *43*, 58–70. [CrossRef]
2. Dagger, T.; Meier, V.; Hildebrand, S.; Brüggemann, D.; Winter, M.; Schappacher, F.M. Safety Performance of 5 Ah Lithium Ion Battery Cells Containing the Flame Retardant Electrolyte Additive (Phenoxy) Pentafluorocyclotriphosphazene. *Energy Technol.* **2018**, *6*, 2001–2010. [CrossRef]
3. Xu, H.Y.; Xie, S.; Wang, Q.Y.; Yao, X.L.; Wang, Q.S.; Chen, C.H. Electrolyte additive trimethyl phosphite for improving electrochemical performance and thermal stability of $LiCoO_2$ cathode. *Electrochim. Acta* **2006**, *52*, 636–642. [CrossRef]
4. Xiang, H.F.; Jin, Q.Y.; Chen, C.H.; Ge, X.W.; Guo, S.; Sun, J.H. Dimethyl methylphosphonate-based nonflammable electrolyte and high safety lithium–ion batteries. *J. Power Sources* **2007**, *174*, 335–341. [CrossRef]
5. Wang, X.; Yasukawa, E.; Kasuya, S. Nonflammable trimethyl phosphate solvent-containing electrolytes for lithium-ion batteries: I. fundamental properties. *J. Electrochem. Soc.* **2001**, *148*. [CrossRef]

6. Yeh, F.-M.; Volli, V.; Laiwang, B.; Tung, P.-H.; Shu, C.-M. Oxidative stability and thermal performance of ester based lube oil with lithium salt additives. *Appl. Therm. Eng.* **2019**, *150*, 1328–1336. [CrossRef]
7. Li, Y.; An, Y.; Tian, Y.; Fei, H.; Xiong, S.; Qian, Y.; Feng, J. Stable and Safe Lithium Metal Batteries with Ni-Rich Cathodes Enabled by a High Efficiency Flame Retardant Additive. *J. Electrochem. Soc.* **2019**, *166*, A2736–A2740. [CrossRef]
8. Wang, Q.; Sun, J.; Chen, C. Enhancing the thermal stability of LiCoO2 electrode by 4–isopropyl phenyl diphenyl phosphate in lithium ion batteries. *J. Power Sources* **2006**, *162*, 1363–1366. [CrossRef]
9. Yao, X.L.; Xie, S.; Chen, C.H.; Wang, Q.S.; Sun, J.H.; Li, Y.L.; Lu, S.X. Comparative study of trimethyl phosphite and trimethyl phosphate as electrolyte additives in lithium ion batteries. *J. Power Sources* **2005**, *144*, 170–175. [CrossRef]
10. Wang, W.; Liao, C.; Liu, L.; Cai, W.; Yuan, Y.; Hou, Y.; Guo, W.; Zhou, X.; Qiu, S.; Song, L.; et al. Comparable investigation of tervalent and pentavalent phosphorus based flame retardants on improving the safety and capacity of lithium-ion batteries. *J. Power Sources* **2019**, *420*, 143–151. [CrossRef]
11. Liu, L.; Du, C.; Wang, S.; Chen, S. Three new bifunctional additives for safer nickel-cobalt-aluminum based lithium ion batteries. *Chin. Chem. Lett.* **2018**, *29*, 1781–1784. [CrossRef]
12. Hyung, Y.E.; Vissers, D.R.; Amine, K. Flame-retardant additives for lithiumion batteries. *J. Power Sources* **2003**, *119–121*, 383–387. [CrossRef]
13. Xia, L.; Xia, Y.; Liu, Z. A novel fluorocyclophosphazene as bifunctional additive for safer lithium-ion batteries. *J. Power Sources* **2015**, *278*, 190–196. [CrossRef]
14. Liu, J.; Song, X.; Zhou, L.; Wang, S.; Song, W.; Liu, W.; Long, H.; Zhou, L.; Wu, H.; Feng, C.; et al. Fluorinated phosphazene derivative—A promising electrolyte additive for high voltage lithium ion batteries: From electrochemical performance to corrosion mechanism. *Nano Energy* **2018**, *46*, 404–414. [CrossRef]
15. Li, X.; Li, W.; Chen, L.; Lu, Y.; Su, Y.; Bao, L.; Wang, J.; Chen, R.; Chen, S.; Wu, F. Ethoxy (pentafluoro) cyclotriphosphazene (PFPN) as a multi-functional flame retardant electrolyte additive for lithium-ion batteries. *J. Power Sources* **2018**, *378*, 707–716. [CrossRef]
16. Huang, A.-C.; Huang, C.-F.; Tang, Y.; Xing, Z.-X.; Jiang, J.-C. Evaluation of multiple reactions in dilute benzoyl peroxide concentrations with additives using calorimetric technology. *J. Loss Prev. Process Ind.* **2021**, *69*, 104373–104378. [CrossRef]
17. Wang, Q.; Liu, S.-H.; Huang, A.-C.; Huang, C.-F.; Chuang, Y.-K.; Shu, C.-M. Effects of mixing malic acid and salicylic acid with metal oxides in medium- to low-temperature isothermal conditions, as determined using the thermal activity monitor IV. *J. Therm. Anal. Calorim.* **2018**, *133*, 779–784. [CrossRef]
18. Huang, A.-C.; Liao, F.-C.; Huang, C.-F.; Tang, Y.; Zhang, Y.; Shu, C.-M.; Xing, Z.-X.; Jiang, J.-C.; Hsieh, W.-Y. Calorimetric approach to establishing thermokinetics for cosmeceutical benzoyl peroxides containing metal ions. *J. Therm. Anal. Calorim.* **2021**, *144*, 373–382. [CrossRef]
19. Yang, Y.P.; Huang, A.C.; Tang, Y.; Liu, Y.C.; Wu, Z.H.; Zhou, H.L.; Li, Z.P.; Shu, C.M.; Jiang, J.C.; Xing, Z.X. Thermal Stability Analysis of Lithium-Ion Battery Electrolytes Based on Lithium Bis(trifluoromethanesulfonyl)imide-Lithium Difluoro(oxalato)Borate Dual-Salt. *Polymers* **2021**, *13*, 707. [CrossRef]
20. Uhlemann, M.; Madian, M.; Leones, R.; Oswald, S.; Maletti, S.; Eychmuller, A.; Mikhailova, D. In-Depth Study of Li4Ti5O12 Performing beyond Conventional Operating Conditions. *ACS Appl. Mater. Interfaces* **2020**, *12*, 37227–37238. [CrossRef]
21. Dagger, T.; Lürenbaum, C.; Schappacher, F.M.; Winter, M. Electrochemical performance evaluations and safety investigations of pentafluoro(phenoxy)cyclotriphosphazene as a flame retardant electrolyte additive for application in lithium ion battery systems using a newly designed apparatus for improved self-extinguishing time measurements. *J. Power Sources* **2017**, *342*, 266–272. [CrossRef]
22. Yan, P.; Zhu, Y.; Pan, X.; Ji, H. A novel flame-retardant electrolyte additive for safer lithium-ion batteries. *Int. J. Energy Res.* **2020**, *45*, 2776–2784. [CrossRef]
23. Lang, P.; Wojcik, T.; Povoden-Karadeniz, E.; Falahati, A.; Kozeschnik, E. Thermo-kinetic prediction of metastable and stable phase precipitation in Al–Zn–Mg series aluminium alloys during non-isothermal DSC analysis. *J. Alloys Compd.* **2014**, *609*, 129–136. [CrossRef]
24. Geng, P.; Zore, A.; Van De Mark, M.R. Thermodynamic characterization of free and surface water of colloidal unimolecular polymer (CUP) particles utilizing DSC. *Polymers (Basel)* **2020**, *12*, 1417. [CrossRef] [PubMed]
25. Huang, A.-C.; Huang, C.-F.; Xing, Z.-X.; Jiang, J.-C.; Shu, C.-M. Thermal hazard assessment of the thermal stability of acne cosmeceutical therapy using advanced calorimetry technology. *Process Saf. Environ. Prot.* **2019**, *131*, 197–204. [CrossRef]
26. Tsai, Y.T.; Yang, Y.; Huang, H.C.; Shu, C.M. Inhibitory effects of three chemical dust suppressants on nitrocellulose dust cloud explosion. *AlChE J.* **2020**, *66*, 16888–16899. [CrossRef]
27. Tahmasebi, A.; Yu, J.; Su, H.; Han, Y.; Lucas, J.; Zheng, H.; Wall, T. A differential scanning calorimetric (DSC) study on the characteristics and behavior of water in low-rank coals. *Fuel* **2014**, *135*, 243–252. [CrossRef]
28. Cucos, A.; Budrugeac, P.; Miu, L. DMA and DSC studies of accelerated aged parchment and vegetable–tanned leather samples. *Thermochim. Acta* **2014**, *583*, 86–93. [CrossRef]
29. Duh, Y.-S.; Ho, T.-C.; Chen, J.-R.; Kao, C.-S. Study on exothermic oxidation of acrylonitrile-butadiene-styrene (ABS) resin powder with application to ABS processing safety. *Polymers* **2010**, *2*, 174–187. [CrossRef]
30. Tsai, Y.T.; Huang, G.T.; Zhao, J.Q.; Shu, C.M. Dust cloud explosion characteristics and mechanisms in MgH2 based hydrogen storage materials. *AlChE J.* **2021**. [CrossRef]

31. Wu, W.-Q.; Feng, W.; Lin, Q.-H.; Wang, S.-Y.; Guo, Z.-C.; Chen, L.-P.; Chen, W.-H. Synthesis and thermal decomposition of TNPG. *Thermochim. Acta* **2020**, *683*, 178396. [CrossRef]
32. Vyazovkin, S. Kissinger method in kinetics of materials: Things to beware and be aware of. *Molecules* **2020**, *25*, 2813. [CrossRef] [PubMed]
33. Vyazovkin, S.; Burnham, A.K.; Criado, J.M.; Pérez-Maqueda, L.A.; Popescu, C.; Sbirrazzuoli, N. ICTAC Kinetics Committee recommendations for performing kinetic computations on thermal analysis data. *Thermochim. Acta* **2011**, *520*, 1–19. [CrossRef]
34. Ferrer, N.; Serra, E.; Sempere, J.; Nomen, R. Non-parametric kinetic analysis of autocatalytic reactions. *J. Loss Prev. Process Ind.* **2017**, *49*, 357–366. [CrossRef]
35. Deng, J.; Zhao, J.-Y.; Huang, A.-C.; Zhang, Y.-N.; Wang, C.-P.; Shu, C.-M. Thermal behavior and microcharacterization analysis of second-oxidized coal. *J. Therm. Anal. Calorim.* **2017**, 439–448. [CrossRef]
36. Farjas, J.; Roura, P. Exact analytical solution for the Kissinger equation: Determination of the peak temperature and general properties of thermally activated transformations. *Thermochim. Acta* **2014**, *598*, 51–58. [CrossRef]
37. Tankov, I.; Yankova, R.; Mitkova, M.; Stratiev, D. Non-isothermal decomposition kinetics of pyridinium nitrate under nitrogen atmosphere. *Thermochim. Acta* **2018**, *665*, 85–91. [CrossRef]
38. Bianchi, O.; Oliveira, R.V.B.; Fiorio, R.; De Martins, J.N.; Zattera, A.J.; Canto, L.B. Assessment of Avrami, Ozawa and Avrami–Ozawa equations for determination of EVA crosslinking kinetics from DSC measurements. *Polym. Test.* **2008**, *27*, 722–729. [CrossRef]
39. Vyazovkin, S.; Sbirrazzuoli, N. Isoconversional kinetic analysis of thermally stimulated processes in polymers. *Macromol. Rapid Commun.* **2006**, *27*, 1515–1532. [CrossRef]
40. Zhang, Z.; Wang, C.; Huang, G.; Liu, H.; Yang, S.; Zhang, A. Thermal degradation behaviors and reaction mechanism of carbon fibre-epoxy composite from hydrogen tank by TG-FTIR. *J. Hazard. Mater.* **2018**, *357*, 73–80. [CrossRef]
41. Campion, C.L.; Li, W.; Lucht, B.L. Thermal decomposition of LiPF6-based electrolytes for lithium-ion batteries. *J. Electrochem. Soc.* **2005**, *152*, 35–42. [CrossRef]
42. Sloop, S.E.; Pugh, J.K.; Wang, S.; Kerr, J.B.; Kinoshita, K. Chemical reactivity of PF5 and LiPF6 in ethylene carbonate/dimethyl carbonate solutions. *Electrochem. Solid State Lett.* **2001**, *4*, 357–364. [CrossRef]
43. Venkatesh, M.; Ravi, P.; Tewari, S.P. Isoconversional kinetic analysis of decomposition of nitroimidazoles: Friedman method vs. Flynn–Wall–Ozawa method. *J. Phys. Chem. A* **2013**, *117*, 10162–10181. [CrossRef] [PubMed]
44. El Hazzat, M.; Sifou, A.; Arsalane, S.; El Hamidi, A. Novel approach to thermal degradation kinetics of gypsum: Application of peak deconvolution and Model-Free isoconversional method. *J. Therm. Anal. Calorim.* **2019**, *140*, 657–671. [CrossRef]